JACS
JOURNAL OF THE AMERICAN CHEMICAL SOCIETY
Article
pubs.acs.org/JACS

Mechanisms of *syn*-Insertion of Alkynes and Allenes into Gold–Silicon Bonds: A Comprehensive Experimental/Theoretical Study

Maximilian Joost,[†,‡,⊥] Laura Estevez,[§,∥,⊥] Sonia Mallet-Ladeira,[⊥] Karinne Miqueu,*[,§] Abderrahmane Amgoune,*[,†,‡] and Didier Bourissou*[,†,‡]

[†]Université de Toulouse, UPS, Laboratoire Hétérochimie Fondamentale Appliquée, 118 route de Narbonne, F-31062 Toulouse, France

[‡]CNRS, LHFA UMR 5069, F-31062 Toulouse, France

[§]Institut Pluridisciplinaire de Recherche sur l'Environnement et les Matériaux (UMR 5254), Equipe Chimie Physique, Université de Pau et des Pays de l'Adour, Hélioparc, 2 Avenue du Président Angot, 64053 Pau cedex 09, France

[∥]Departamento de Química Física, Universidade de Vigo, Facultade de Química Lagoas-Marcosende s/n, 36310 Vigo, Galicia, Spain

[⊥]Université de Toulouse, UPS, Structure Fédérative Toulousaine en Chimie Moléculaire, FR2599, 118 Route de Narbonne, F-31062 Toulouse, France

Supporting Information

ABSTRACT: A detailed mechanistic study is reported for the *syn*-insertion of alkynes and allenes in the Au–Si bonds of complexes $(R_3P)Au–SiR'Ph_2$ (R = Ph, Me and R′ = *t*-Bu, Ph). Kinetic experiments indicate that (*i*) the reaction is first-order in alkyne and gold silyl complex and (*ii*) it requires a rather low enthalpy of activation and a relatively large negative entropy of activation [$\Delta H^{‡}$ = 13.7 (±1.6) kcal·mol^{-1} and $\Delta S^{‡}$ = −32.0 (±5.0) cal·mol^{-1}·K^{-1} for the reaction of $(Ph_3P)Au–Si(t\text{-Bu})Ph_2$ with methyl propiolate], in line with a bimolecular associative transformation. The different mechanistic pathways have been explored by DFT calculations. Accordingly, the reaction is found to proceed via a two-step inner-sphere mechanism: (*i*) first, the alkyne coordinates to the gold silyl complex to form a π-complex; (*ii*) the subsequent migratory insertion step is rate determining and occurs in a concerted manner. Provided dispersion effects are taken into account (B97D functional), the enthalpy of activation estimated theoretically [$\Delta H^{‡}$ = 11.5 kcal·mol^{-1}] is in good agreement with that measured experimentally. The influence of the π substrate (methyl propiolate, dimethyl acetylene dicarboxylate, phenyl acetylene, ethyl 2,3-butadienoate) has been analyzed theoretically, and the regioselectivity of the insertion has been rationalized. In particular, the unexpected selectivity observed experimentally with the allene is shown to result from the insertion of the terminal nonactivated C=C double bond into the Au–Si bond of $(Ph_3P)Au–SiPh_3$, followed by an original isomerization (Au/Si exchange process). This study provides unambiguous evidence for coordination–insertion at gold and thereby strongly supports the possible occurrence of inner-sphere mechanisms during the functionalization of alkynes and allenes.

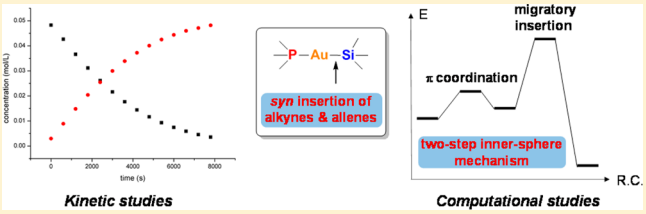

INTRODUCTION

Due to their excellent carbophilic Lewis acidity combined with the unique functional group tolerance, gold complexes are very powerful catalysts for the activation of CC multiple bonds toward nucleophilic attack. Over the past 15 years, a broad variety of valuable catalytic transformations have been developed on this basis.[1] In parallel, a thorough understanding of the reactivity of gold complexes toward π-systems has been gained thanks to experimental studies and high-level computational analyses.[2]

The addition of nucleophiles to alkynes, alkenes, and allenes catalyzed by gold typically proceeds in a stepwise manner. The first step is the activation of the π-substrate upon side-on coordination to a cationic gold center. Such π-complexes of gold have been extensively investigated, and the data collected experimentally and computationally provide a detailed picture of their structure and properties.[3] Note that the ability of gold to doubly activate terminal alkynes and form (σ,π) dinuclear complexes has also been recently substantiated, which opens new synthetic avenues.[4] In a second step, a nucleophile adds to the π-complex *anti* to gold, affording a vinyl gold complex with *trans* arrangement of the incoming nucleophile and gold center (Figure 1). The vinyl gold complex can eventually react further or directly liberate the functionalized substrate, most commonly via protodeauration.

Another pathway may also be envisioned for the reaction of nucleophiles on π-systems upon gold activation. Instead of *anti* nucleophilic attack on a π-complex, it involves coordination of the nucleophile to gold and then *syn*-insertion of the π-substrate into the Au–Nu bond. This inner-sphere mechanism leads to *cis* vinyl gold complexes.

Received: April 22, 2014
Published: July 7, 2014

   dx.doi.org/10.1021/ja504024h | J. Am. Chem. Soc. 2014, 136, 10373–10382

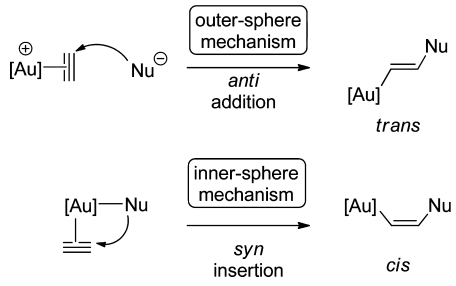

Figure 1. Formation of vinyl gold complexes from alkynes: schematic representation of the outer- and inner-sphere mechanisms.

The dichotomy between outer/inner-sphere mechanisms has been frequently discussed in gold catalysis, in particular in the frame of hydration,[5] alkoxylation,[6] and amination[7] reactions.[8] The outer-sphere mechanism has been supported by several experimental observations and computational studies.[9−13] Conversely, no direct unambiguous evidence for the inner-sphere mechanism has been reported to date,[14] and in fact, the ability of gold complexes to lead to *syn* insertion products has only been recently substantiated.[15,16]

Last year, we reported that gold(I) silyl complexes readily react with unsaturated substrates, leading to isolable β-silyl vinyl gold complexes.[17,18] Terminal and internal alkynes, as well as allenes were shown to insert into Au−Si bonds in a stereo- and regioselective manner. This unprecedented reactivity for gold prompted us to carry out a detailed experimental/computational mechanistic study that we report hereafter. Kinetic experiments using multinuclear NMR monitoring have been performed to determine the rate law and activation parameters. The various possible mechanistic pathways have been explored computationally (DFT calculations using different density functionals), and the influence of the substrate (methyl propiolate, dimethyl acetylene dicarboxylate, phenyl acetylene, ethyl 2,3-butadienoate) has been analyzed. These studies provide a detailed picture of the reaction mechanism and substantiate a two-step inner-sphere pathway involving coordination of the π-system followed by *syn* insertion into the Au−Si bond. They also point out the involvement of an original isomerization process in the case of ethyl 2,3-butadienoate which explains the unexpected regioselectivity observed experimentally.

RESULTS AND DISCUSSION

Kinetic Studies of the Reaction between the Gold Silyl Complex 1 and Methyl Propiolate. Treatment of the gold silyl complex **1** with methyl propiolate (MP) gives the vinyl gold complex **2** with complete stereo- and regioselectivity. Kinetic experiments were performed in NMR tubes (in C_6D_6, using 10 equiv of MP per gold complex). ^{1}H NMR monitoring shows the progressive formation of complex **2** without a detectable intermediate (Scheme 1). The respective concentrations of the reactants and product were followed over time by integrating the resonance signals corresponding to the OCH_3 moiety of MP (δ = 3.12 ppm), the *t*-Bu group of complex **1** (δ = 1.50 ppm), and the vinylic proton of complex **2** (δ = 8.40 ppm). According to kinetic plots (a) and (b), the consumption of the gold silyl complex **1** follows a first-order decay and the reaction is overall second-order (see Supporting Information for details). Thus, the reaction is first-order with respect to each reactant (rate law: $v = k_{obs}[\mathbf{1}][MP]$), in line with a bimolecular process.[19]

The rate constant k_{obs} was determined at different temperatures (25 to 65 °C, 10 °C steps), and the activation parameters were extracted from the corresponding Eyring plot. Accordingly, the insertion reaction was found to require a rather low enthalpy of activation, $\Delta H^{\ddagger}$ = 13.7 (±1.6) kcal·mol^{-1}. The entropy of activation is negative and relatively large, $\Delta S^{\ddagger}$ = −32.0 (±5.0) cal/(mol·K), in agreement with an associative mechanism. Overall, the enthalpic and entropic terms contribute about equally to the Gibbs free energy of activation, $\Delta G^{\ddagger}$ = 24.4 (±2.3) kcal·mol^{-1} at 60 °C.

Reactions of alkynes with transition metal complexes eventually display secondary kinetic isotope effects (KIE) as a consequence of the change in hybridization from C_{sp} to C_{sp^2} in the rate-determining step.[20] Thus, methylpropiolate H/D labeling studies have been carried out and ^{1}H NMR spectroscopy indicated a negligible kinetic isotope effect [k_H/k_D = 1.04 (±0.06)] in this case (see Supporting Information for details).

Computational Study of the Reaction between the Gold Silyl Complex 1 and Methyl Propiolate. Two plausible pathways may be considered to explain the formation of the *syn* insertion complex **2**: (*i*) a one-step 1,2 addition of the gold silyl complex **1** to the CC triple bond of MP or (*ii*) a two-

Scheme 1. Reaction of Complex 1 with Methylpropiolate Monitored by ^{1}H NMR Spectroscopy[a]

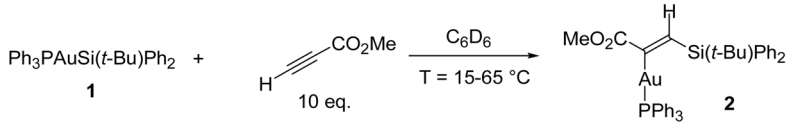

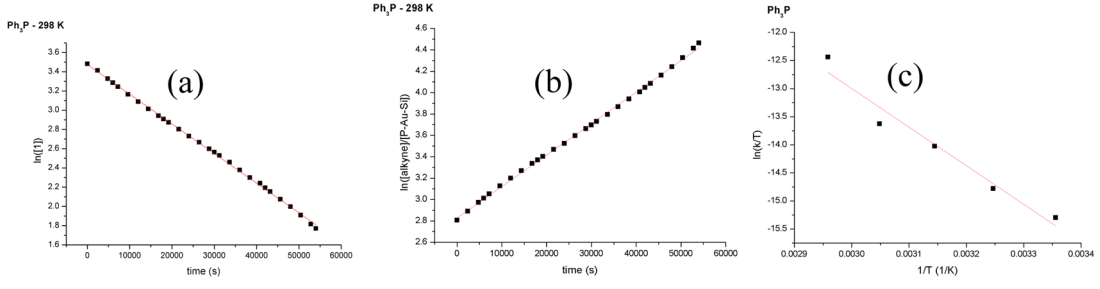

[a]C_6D_6, $[\mathbf{1}]_0$ = 0.0483 mol/L, $[\mathbf{MP}]_0$ = 0.483 mol/L. (a) Plot of ln[**1**] *vs* time (s). (b) Plot of ln([MP]/[**1**]) *vs* time (s). (c) Plot of ln(k_{obs}/T) *vs* 1/*T* (K^{-1}) (temperature range: 25−65 °C).

dx.doi.org/10.1021/ja504024h | J. Am. Chem. Soc. 2014, 136, 10373−10382

step pathway involving coordination of the alkyne to gold followed by a migratory insertion process. Both mechanisms were investigated by DFT calculations (B97D density functional)[21] on the actual reaction, *i.e.* without simplification of the reactants.

1,2 Addition Pathway. The potential energy surface (PES) was scrutinized to localize a transition state (TS) accounting for a direct 1,2 addition of the Au−Si bond to the alkyne. Optimizations from diverse starting geometries (Au−C1 and Si−C2 bond distances ranging from 1.90 to 2.35 Å) did not allow the localization of the expected in-plane (Au,Si,C1,C2) four-center transition state structure. In fact, the only way to find a transition state (TS) corresponding to the addition of the Au−Si bond to MP was by decoordinating the PPh_3 ligand from gold (Scheme 2). Phosphine dissociation is not very

Scheme 2. 1,2 Addition of the Au−Si Bond to Methyl Propiolate (with and without PPh_3 Dissociation)

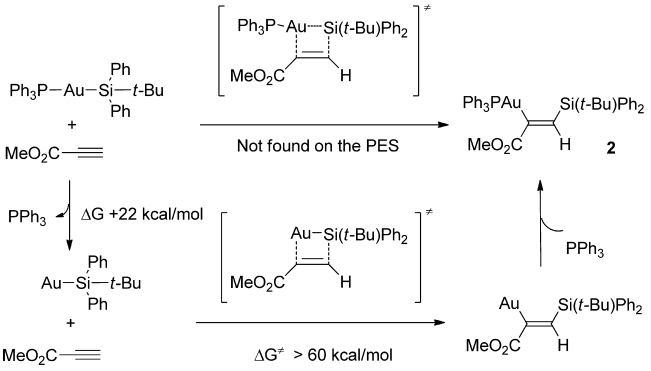

costly in energy (it is endergonic by 22.0 kcal·mol^{-1}), but the ensuing transition state for 1,2 addition is prohibitively high in energy ($\Delta G^{\ddagger}$ = 64.6 kcal·mol^{-1}, $\Delta H^{\ddagger}$ = 63.0 kcal·mol^{-1}). It is thus very unlikely that complex **2** is formed by 1,2 addition of the Au−Si bond to MP (Figure S19).

Coordination−Insertion Pathway. While no in-plane TS could be localized on the PES for the reaction of **1** with MP, an out-of-plane four-center transition state $\mathbf{TS_{1\to2}}$ associated with the insertion of the alkyne into the Au−Si bond of **1** was identified. Intrinsic Reaction Coordinate (IRC) calculations indicate that $\mathbf{TS_{1\to2}}$ is connected to the vinyl gold complex **2** and to a π-adduct $\boldsymbol{\pi_{1\to2}}$ between MP and **1** (Figure 2). The $\boldsymbol{\pi_{1\to2}}$ intermediate species is slightly higher in energy than the free reactants (ΔG = 5.2 kcal·mol^{-1}), and its formation requires a low activation barrier ($\Delta G^{\ddagger}$ = 8.3 kcal·mol^{-1}). Altogether, this leads to a two-step coordination−insertion mechanism for the formation of the vinyl gold complex **2**. The reaction is thermodynamically favored (overall Gibbs energy ΔG = −31.4 kcal·mol^{-1}), and the rate-determining step is the insertion of the alkyne into the Au−Si bond ($\Delta G^{\ddagger}_{1\to2}$ = 30.1 kcal·mol^{-1}).

At this stage, several density functionals (B97D, M06, B3PW91) were evaluated in order to determine the most appropriate method (Table S4). With the B3PW91 functional, the value predicted for $\Delta H^{\ddagger}_{1\to2}$ is overestimated by 10 kcal·mol^{-1} compared to that determined experimentally (13.7 kcal·mol^{-1}). Significantly better results were obtained with B97D and M06, two density functionals taking into account dispersion interactions.[22] In this case, the values computed for $\Delta H^{\ddagger}_{1\to2}$ (11.5 and 14.2 kcal·mol^{-1}, respectively) deviate by less than 2.5 kcal·mol^{-1} from that estimated by ^{1}H NMR. These results

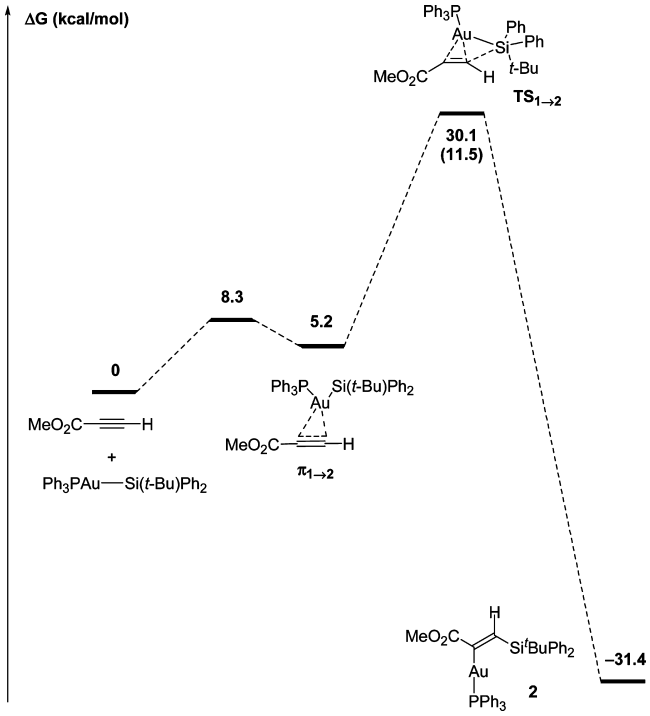

Figure 2. Reaction profile for the insertion of methyl propiolate into the Au−Si bond of the gold silyl complex **1** (ΔG in kcal·mol^{-1}), computed at the B97D/SDD+f(Au)-6-31G** level of theory. Enthalpy of activation $\Delta H^{\ddagger}$ (in kcal·mol^{-1}) in parentheses.

emphasize the importance of noncovalent interactions in such systems which are relatively large (with 43 non-hydrogen atoms) and feature main group elements (P,Si) as well as a gold center. Note that the value computed for $\Delta G^{\ddagger}_{1\to2}$ is systematically overestimated, the best match being found with the B97D functional (predicted: 30.1 kcal·mol^{-1}, experimentally determined: 23.2 kcal·mol^{-1} at 298 K). These deviations arise from the difficulty in estimating accurately the entropic contribution, which is especially challenging for reactions involving a change in molecularity.[23] Overall, the B97D functional offers the best comprise in terms of accuracy vs computing time, and it was thus preferred for the following calculations.

The structures of the key stationary points were then examined thoroughly, starting from the intermediate π-complex (Figure 3). The optimized geometry of $\boldsymbol{\pi_{1\to2}}$ indicates that methyl propiolate binds to gold in a side-on fashion and lies in the same coordination plane as phosphorus and silicon. Upon coordination, the CC triple bond elongates by 0.07 Å and the P−Au−Si framework bends significantly (104.7°). Also interesting to note is the nonsymmetric coordination of the alkyne, the Au−C1 distance being substantially shorter than the Au−C2 distance (2.108 Å vs 2.267 Å). To shed light on the bonding situation, the molecular orbitals of $\boldsymbol{\pi_{1\to2}}$ were analyzed. Accordingly, the main interaction between **1** and MP (Figure S20) involves the HOMO of the gold silyl complex (a combination of σ_{AuSi} and $d_{yz(Au)}$ orbitals) and the LUMO of methyl propiolate ($\pi^*_{C\equiv C}$). NPA charges calculated from Natural Bond Order analysis (NBO) also revealed a net charge transfer of 0.47 e− from the gold silyl complex **1** to methyl propiolate (Table S6). The bonding situation found in $\boldsymbol{\pi_{1\to2}}$ differs from that observed upon coordination of alkynes to (L)Au$^+$ fragments.[3] For example, upon coordination of MP to

dx.doi.org/10.1021/ja504024h | J. Am. Chem. Soc. 2014, 136, 10373−10382

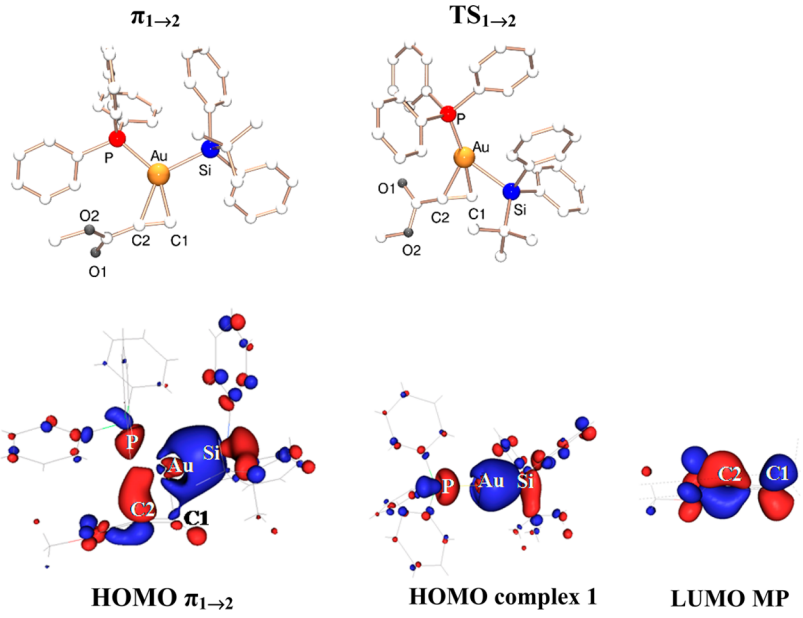

Figure 3. (Top) Intermediate $\pi_{1\to2}$ and transition state $TS_{1\to2}$ computed for the insertion of methyl propiolate into the Au−Si bond of **1**. Selected bond distances (Å) and angles (deg): $\pi_{1\to2}$: AuC1, 2.108; AuC2, 2.267; C1C2, 1.280; AuSi, 2.405; AuP, 2.395; PAuSi, 104.7; $TS_{1\to2}$: AuC1, 2.125; AuC2, 2.318; C1C2, 1.323; AuSi, 2.587; AuP, 2.273; C1Si, 2.357; PAuSi, 130.8. (Bottom) Plots of the HOMO of intermediate $\pi_{1\to2}$ and corresponding fragment orbitals (±0.04 au isosurfaces). B97D/SDD+f(Au)-6-31G** level of theory.

$(Ph_3P)Au^+$, there is a net charge transfer of 0.12 e− from the alkyne to the metal fragment, and the main orbital interaction involves the HOMO of MP ($\pi_{C\equiv C}$) and the LUMO of $(Ph_3P)Au^+$ (σ^*_{PAu}) (Figures S20 and S21).

The structure of the transition state $TS_{1\to2}$ corresponding to the insertion step was then studied. Starting from $\pi_{1\to2}$, the reaction involves migration of the silyl group from Au to C1 with a concomitant shift of gold toward C2, resulting overall in the *syn* insertion of MP into the Au−Si bond. The most important geometrical modifications from $\pi_{1\to2}$ to $TS_{1\to2}$ are (*i*) the displacement of the silyl group out of the (Au,C1,C2) plane (C1C2AuSi = −34.5° in $TS_{1\to2}$ vs −7.0° in $\pi_{1\to2}$) and (*ii*) the widening of the P−Au−Si bond angle (130.8°), which altogether bring the Si atom close to C1 (SiC1 = 2.357 Å). It is also interesting to note that, from an electronic point of view, the charge transfer from **1** to MP increases further by 0.33 au in $TS_{1\to2}$.

Note also that the C1 atom already develops sp^2 character in $\pi_{1\to2}$ (the AuC1 bond is short at 2.125 Å and the C1C2H bond angle is significantly bent at 146°) and thus does not experience a significant change in hybridization in the rate-determining step. This is consistent with the negligible KIE observed experimentally.

The formation of the other conceivable regioisomer of the vinyl gold complex **2′** has also been investigated computationally for comparison (*syn* insertion of MP in the Au−Si bond, with the silyl group introduced in the α instead of β position of the CO_2Me substituent). The most favorable pathway to form **2′** is again a two-step coordination−insertion process (Figure S22). The transition state $TS_{1\to2'}$ for the rate-determining step stands 6−7 kcal·mol^{-1} higher in energy than $TS_{1\to2}$ (both in *H* and *G*), and the regioisomer **2′** was found to be less stable than **2** by 4 kcal·mol^{-1} (ΔG = −27.6 kcal·mol^{-1}), in agreement with the selective formation of **2** as observed experimentally.

Reaction between the Gold Silyl Complex 3 and Methyl Propiolate. In order to confirm the conclusions drawn from the reaction of **1** with MP, similar kinetic and computational investigations were performed with complex **3**, featuring PMe_3 instead of PPh_3 at gold. The insertion reaction of MP proceeds faster with **3** than with **1** (1 h vs 8 h at 60 °C) and is again fully stereo- and regioselective, affording the β-silyl vinyl gold complex **4** as the sole product (Scheme 3).

Scheme 3. *Syn* Insertion of Methylpropiolate into Au−Si Bond of Complex 3

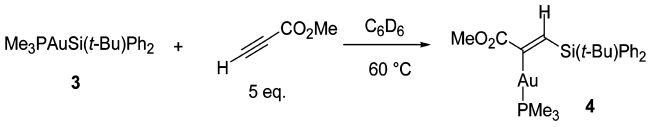

The kinetic data obtained by ^{1}H NMR monitoring of the reaction between **3** and MP (5 equiv) showed here also a first-order dependence in each of the reactants (see Supporting Information). An Eyring plot was obtained from the temperature dependence of the rate constant (15−55 °C), and the following activation parameters were extracted: $\Delta H^‡$ = 14.5 (±0.7) kcal·mol^{-1} (vs 13.7 kcal·mol^{-1} for complex **1**) and $\Delta S^‡$ = −21.4 (±2.3) cal/(mol·K) (vs −32.0 cal/(mol·K) for complex **1**), corresponding to a Gibbs free energy of activation $\Delta G^‡$ of 21.6 kcal·mol^{-1} at 60 °C (that is ∼3 kcal·mol^{-1} lower than that found for **1**, $\Delta G^‡$ = 24.4 kcal·mol^{-1}). The main difference comes from the entropic term which is significantly lower with complex **3**. According to DFT calculations, the reaction proceeds by coordination−insertion and the reaction profile computed for **3** is similar to that found for complex **1** (Figure S24). The enthalpy of activation predicted by DFT ($\Delta H^‡_{3\to4}$ = 13.3 kcal·mol^{-1} with the B97D functional) fits with that determined experimentally (Table S5). Moreover, the intermediate π-complex $\pi_{3\to4}$ and transition state $TS_{3\to4}$ for the insertion step display similar structures to those for $\pi_{1\to2}$ and $TS_{1\to2}$. The prevailing orbital interaction arises from the HOMO of the gold silyl complex ($\sigma_{AuSi}/d_{yz(Au)}$ combination) and the LUMO of methyl propiolate ($\pi^*_{C\equiv C}$), and it is

dx.doi.org/10.1021/ja504024h | *J. Am. Chem. Soc.* 2014, 136, 10373−10382

Scheme 4. Competitive Insertion of Dimethyl Acetylene Dicarboxylate in the Au−Si and Au−P Bonds of the Phosphine Gold Silyl Complex 1

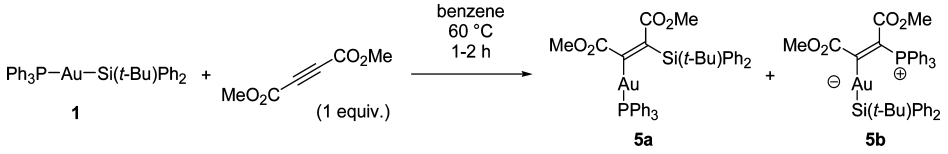

associated with a substantial charge transfer from **3** to MP (by 0.54e− au in $\pi_{3\rightarrow4}$ according to NBO charges).

Thus, the reaction of complex **3** with MP corroborates the results obtained with **1** and the two-step coordination−insertion process seems decidedly favored over other conceivable mechanistic pathways. The gold silyl complexes **1** and **3** first react with methyl propiolate to give π-complexes. The subsequent insertion step is rate determining and occurs in a concerted manner (migration of the silyl group from Au to C1 with a concomitant shift of Au toward C2, resulting in *syn* insertion of MP in the Au−Si bond). The regioselectivity of the reaction is well-reproduced theoretically and follows the polarity of the alkyne, with a preference for the silyl group to attack MP at the terminal electrophilic carbon atom (Michael-type addition).

The reaction between (Ph_3P)AuMe and methylpropiolate (MP) was investigated for comparison. Computationally, the reaction was predicted to also proceed via a two-step inner-sphere mechanism (Figure S25). It is thermodynamically favored (ΔG = −36.8 kcal·mol^{-1}), but the rate determining insertion step requires a significantly higher activation barrier ($\Delta G^{\ddagger}$ = 40.3 kcal·mol^{-1}, ∼10 kcal·mol^{-1} higher than the one found for the gold-silyl complex **1**). Analysis of the molecular orbitals revealed that the main interaction between the (Ph_3P)AuMe complex and MP in the π-complex and in the TS also involves the HOMO of the gold complex (σ_{AuC} orbital) and the LUMO of the alkyne ($\pi^*_{C=C}$ orbital) (Figure S26). The HOMO of the Au−Me complex is lower in energy than that of the gold silyl complex **1** (by 0.4 ev), and thus the HOMO−LUMO gap increases. Accordingly, the charge transfer from the Au−Me complex to MP at the TS is significantly lower than that computed for the Au−Si complex (0.80 e$^-$ for Au−Si vs. 0.53 e$^-$ for Au−Me). In line with computational studies, no reaction was observed experimentally between the (Ph_3P)AuMe complex and MP under the same conditions compared to the silyl complexes (60 °C, several hours). All attempts to carry out the reaction at higher temperatures or during prolonged reaction times resulted only in the decomposition of the (Ph_3P)AuMe complex.

Influence of the Alkyne on the Reaction of Gold Silyl Complexes. In order to probe the influence of the alkyne on reactivity and selectivity, we then investigated the reaction of complex **1** with a more activated alkyne than MP, namely dimethyl acetylenedicarboxylate (DMAD), and a less activated alkyne than MP, namely phenyl acetylene (PA).

Reaction of the Phosphine Gold Silyl Complex 1 with Dimethyl Acetylene Carboxylate. Complex **1** readily reacts with DMAD, and complete conversion is achieved within 1−2 h at 60 °C using only 1 equiv of the alkyne (Scheme 4). As expected, the reaction yields the vinyl gold complex **5a** as the result of *syn* insertion of DMAD in the Au−Si bond of **1**. However, ^{31}P NMR monitoring indicates the concomitant formation of a second complex **5b** exhibiting a resonance signal at significantly higher field (δ = 16.1 ppm for **5b** vs 40 ppm for **5a**). According to ^{31}P NMR, the two species are formed in approximately equal amounts. After workup, the compounds were isolated in pure form and their structures were unambiguously ascertained by spectroscopic and crystallographic means (Figure 4). The ^{31}P and ^{29}Si NMR data of

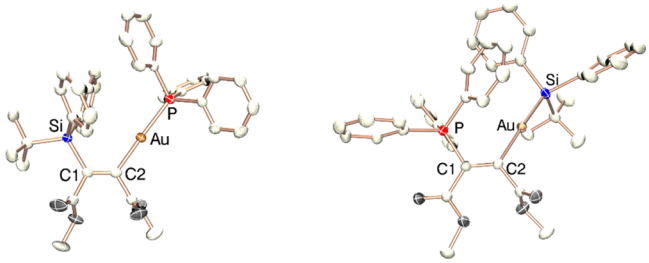

Figure 4. Molecular views of complexes **5a** (left) and **5b** (right) in the solid state (thermal ellipsoids set at 50% probability; hydrogen atoms and solvent molecules are omitted for clarity).

complex **5b** are very different from those of the vinyl gold complex **5a**. Interestingly, complex **5b** displays a ^{29}Si NMR resonance signal at δ = 31.4 ppm (vs −7.7 ppm for complex **5b**), very close to that of the starting gold silyl complex **1** (δ = 35.4 ppm), suggesting that the Au−Si bond is retained in **5b**. X-ray diffraction analysis revealed a zwitterionic structure for **5b** that results from the *syn* insertion of DMAD in the Au−P bond (instead of Au−Si bond) of **1**. Interestingly, **5b** slowly converts to **5a** upon prolonged heating (60 °C, overnight), indicating that **5a** is thermodynamically more stable than **5b**.

According to calculations, direct 1,2-addition and coordination−insertion are unlikely to account for the insertion of DMAD into the Au−P bond of **1**.[24] Instead, the reaction profile leading to **5b** was found to involve the dissociation of PPh_3 (ΔG_{diss} = 22.0 kcal·mol^{-1}) from complex **1** (facilitated by the strong *trans* influence of the silyl ligand),[25] followed by Michael addition of PPh_3 to DMAD to form a phosphonium enolate species.[26] Finally, nucleophilic addition of the vinyl anion to the gold silyl fragment affords complex **5b**. Both, the addition of Ph_3P to DMAD and the nucleophilic addition of the vinyl anion to gold silyl are barrierless processes (see Supporting Information for details, Figure S27).

The reaction profile leading to complex **5a** was explored in detail, and as for methyl propiolate, the *syn* insertion of dimethyl acetylene dicarboxylate in the Au−Si bond of **1** proceeds via a two-step coordination−insertion pathway (Figure S28).[27] The formation of the intermediate π-complex $\pi_{1\rightarrow5a}$ is slightly endergonic (ΔG = 3.3 kcal·mol^{-1}), similarly to that found for methyl propiolate (ΔG = 5.2 kcal·mol^{-1}). But the transition state $TS_{1\rightarrow5a}$ corresponding to the rate-determining insertion step is readily accessible in energy, and the activation barrier for the *syn* insertion of DMAD is estimated to $\Delta H^{\ddagger}_{1\rightarrow5a}$ = 3.2 kcal·mol^{-1} ($\Delta G^{\ddagger}_{1\rightarrow5a}$= 22.4 kcal·mol^{-1}). This is about 8 kcal·mol^{-1} lower than with MP and agrees well with the experimental observations (a faster reaction

dx.doi.org/10.1021/ja504024h | J. Am. Chem. Soc. 2014, 136, 10373−10382

of **1** with DMAD than with MP). Overall, the process leading to **5a** is thermodynamically favored (ΔG = −28.0 kcal·mol^{-1}) compared to that leading to **5b** (ΔG = −9.8 kcal/mol), in line with experimental observations.

The molecular structure of $\boldsymbol{\pi}_{\mathbf{1}\rightarrow\mathbf{5a}}$ deserves some comments. Here also the PAuSi fragment is strongly bent (111.4°) and the alkyne coordinates in the PAuSi plane. Despite the symmetric nature of DMAD, the π-complex is dissymmetric ($d_{\mathrm{AuC1}(trans\ \mathrm{to\ P})}$ = 2.132 Å, $d_{\mathrm{AuC2}(trans\ \mathrm{to\ Si})}$ = 2.270 Å) as the result of the stronger *trans* influence of the silyl over the phosphine ligand.[28]

The lower activation barrier found for DMAD compared to MP is consistent with the smaller HOMO(**1**)−LUMO(alkyne) energy gap (the LUMO of DMAD is lower in energy than that of MP by 0.2 eV) and the higher **1** → alkyne charge transfer (0.85 e− au for DMAD vs 0.80 e− for MP, according to NBO charges). The enhanced electro-deficient character of DMAD also favors Michael addition of PPh_3 and probably explains the competitive insertions in the Au−Si and Au−P bond of **1**, while MP selectively inserts in the Au−Si bond.

Reaction of the Phosphine Gold Silyl Complex ***1*** *with Phenyl Acetylene.* We have previously shown that complex **1** reacts with PA to give the corresponding vinyl gold complex **6a** (Scheme 5). As for MP, the reaction proceeds with complete stereo- and regioselectivity but it requires a longer reaction time (3 weeks vs 8 h).

Scheme 5. *Syn* Insertion of Phenyl Acetylene in the Au−Si Bond of the Gold Silyl Complex 1

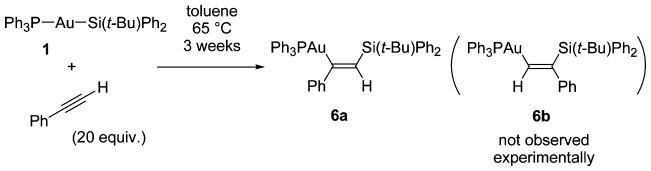

Calculations support a two-step coordination−insertion pathway for the formation of **6a** from **1** and PA (Figure 5). The associated activation barrier amounts to $\Delta H^{\ddagger}_{\mathbf{1}\rightarrow\mathbf{6a}}$ = 21.4 kcal·mol^{-1} ($\Delta G^{\ddagger}_{\mathbf{1}\rightarrow\mathbf{6a}}$ = 39.6 kcal·mol^{-1}). This value is about 10 kcal·mol^{-1} higher than that predicted for MP, in line with experimental observations. The intermediate π-complex $\boldsymbol{\pi}_{\mathbf{1}\rightarrow\mathbf{6a}}$ is also found somewhat uphill in energy ($\Delta G\boldsymbol{\pi}_{\mathbf{1}\rightarrow\mathbf{6a}}$ = 9.8 kcal·mol^{-1}). The overall structures of the intermediate $\boldsymbol{\pi}_{\mathbf{1}\rightarrow\mathbf{6a}}$ and transition state $\mathbf{TS}_{\mathbf{1}\rightarrow\mathbf{6a}}$ are very similar to those observed with MP. The alkyne is dissymmetrically coordinated to gold, the stronger interaction involving the terminal carbon atom. In $\boldsymbol{\pi}_{\mathbf{1}\rightarrow\mathbf{6a}}$, the AuC(H) and AuC(Ph) distances equal 2.148 and 2.387 Å, respectively. The only noticeable difference between PA and MP relates to the magnitude of their interaction with the gold silyl complex **1**. PA forms a slightly looser π-complex than MP (as apparent from the lengthened AuC distances). Consistently, analysis of the frontier molecular orbitals indicates a less favorable HOMO(**1**)−LUMO(alkyne) interaction for PA than for MP (the LUMO of PA is 0.5 eV higher in energy than that of MP). A smaller charge transfer is also found from complex **1** to PA (0.71 e−) than to MP (0.80 e−).

To complete the computational study, the formation of the other regioisomer **6b** (not observed experimentally) was considered. The corresponding intermediate $\boldsymbol{\pi}_{\mathbf{1}\rightarrow\mathbf{6b}}$ adopts a symmetric structure (with essentially equal AuC distances of 2.198 and 2.207 Å) and lies 3.2 kcal·mol^{-1} higher in energy than $\boldsymbol{\pi}_{\mathbf{1}\rightarrow\mathbf{6a}}$. The activation barrier for the insertion of PA leading to **6b** ($\Delta H^{\ddagger}_{\mathbf{1}\rightarrow\mathbf{6b}}$ = 26.0 kcal·mol^{-1}, $\Delta G^{\ddagger}_{\mathbf{1}\rightarrow\mathbf{6b}}$ = 45.6 kcal·mol^{-1}) is substantially larger than that computed for the formation of **6a**, in agreement with the complete regioselectivity observed experimentally.

Reaction of Ethyl 2,3-Butadienoate with Gold Silyl Complexes. We reported previously that the replacement of the Si(*t*-Bu)Ph_2 group by $SiPh_3$ induces a substantial increase in reactivity of the Au−Si bond. Accordingly, complex **7** was found to react readily with ethyl 2,3-butadienoate (EB), affording the gold vinyl complex **8a** as the sole product (Scheme 6). Surprisingly, the insertion reaction involves the terminal nonactivated double bond of the allene, and the silyl group is introduced in the γ-position to the CO_2Et substituent. To gain insight into this rather unexpected selectivity, the mechanism of the reaction between **7** and EB was investigated computationally.

At this stage, it is important to note that allenes have been frequently used in the context of gold-catalyzed π-activation, and computational analyses of the reaction mechanisms have suggested the possible existence of several isomeric structures for the key gold allene complexes.[29] In addition to the classical η^2-allene form, the involvement of η^1-structures (bent allene, planar allylic, and zwitterionic carbene) has been discussed. Insertion of EB into Au−Si bonds may thus be quite different and more complicated than that of alkynes, as studied formerly.

First, we studied the reaction of complex **7** with the terminal C1═C2 bond of the allene, considering the formation of the two regioisomers **8a** and **8b** (Figure 6). In both cases, the insertion reaction is exergonic and occurs via a two-step coordination−insertion pathway.[30] The formation of the vinyl gold complex **8a** ($\Delta G_{\mathbf{7}\rightarrow\mathbf{8a}}$ = −23.1 kcal·mol^{-1}) is thermodynamically favored by 3 kcal·mol^{-1} over the formation of the alkyl gold complex **8b** ($\Delta G_{\mathbf{7}\rightarrow\mathbf{8b}}$ = −20.2 kcal·mol^{-1}), in agreement with experimental observations. The reaction starts by the coordination of the terminal C1═C2 bond of BE to gold, which is endergonic by about 10 kcal·mol^{-1}. The resulting complexes $\boldsymbol{\pi}_{\mathbf{7}\rightarrow\mathbf{8a}}$ and $\boldsymbol{\pi}_{\mathbf{7}\rightarrow\mathbf{8b}}$ adopt η^2-allene structures, and their relative stability is opposite to that of the insertion products **8a**/**8b** ($\boldsymbol{\pi}_{\mathbf{7}\rightarrow\mathbf{8a}}$, leading to the more stable insertion product, is less stable than $\boldsymbol{\pi}_{\mathbf{7}\rightarrow\mathbf{8b}}$ by about 3 kcal·mol^{-1}). The bonding situation is similar in both π-complexes, the main orbital interaction involving the HOMO of the gold silyl complex and the LUMO+1 ($\pi^*_{\mathrm{C1=C2}}$) of the allene (Figure S31). However, their geometric features are slightly different: the allene binds symmetrically in $\boldsymbol{\pi}_{\mathbf{7}\rightarrow\mathbf{8a}}$ (AuC1, 2.200 Å; AuC2, 2.189 Å) whereas the gold center is tilted toward the central carbon atom of EB in $\boldsymbol{\pi}_{\mathbf{7}\rightarrow\mathbf{8b}}$ (AuC1 = 2.381 Å; AuC2 = 2.113 Å).

Careful examination of the transition states associated with the insertion step (Figure 7) revealed important features and striking differences between the two pathways. $\mathbf{TS}_{\mathbf{7}\rightarrow\mathbf{8a}}$ leads to the insertion product obtained experimentally **8a** (vinyl gold complex with the silyl group in γ-position to the CO_2Et substituent). It corresponds to a direct 1,2-insertion of the C1C2 double bond of BE in the Au−Si bond of **7**. In this case, the TS adopts a planar four-membered ring structure. The silyl group migrates from Au to C1 while the gold center shifts toward C2. The process does not involve the adjacent C═CH(CO_2Et) fragment: the C2C3 bond remains short (1.345 Å, vs 1.460 Å for the C1C2 bond), C3 remains trigonal planar (whereas C1 is pyramidalized, sum of the bond angles Σ_α = 348°), and the terminal CH_2/CH(CO_2Et) moieties remain quasi perpendicular (θ = 82.8°). The corresponding activation barrier is very high ($\Delta H^{\ddagger}_{\mathbf{7}\rightarrow\mathbf{8a}}$ = 20.0 kcal·mol^{-1}, $\Delta G^{\ddagger}_{\mathbf{7}\rightarrow\mathbf{8a}}$ =

dx.doi.org/10.1021/ja504024h | J. Am. Chem. Soc. 2014, 136, 10373−10382

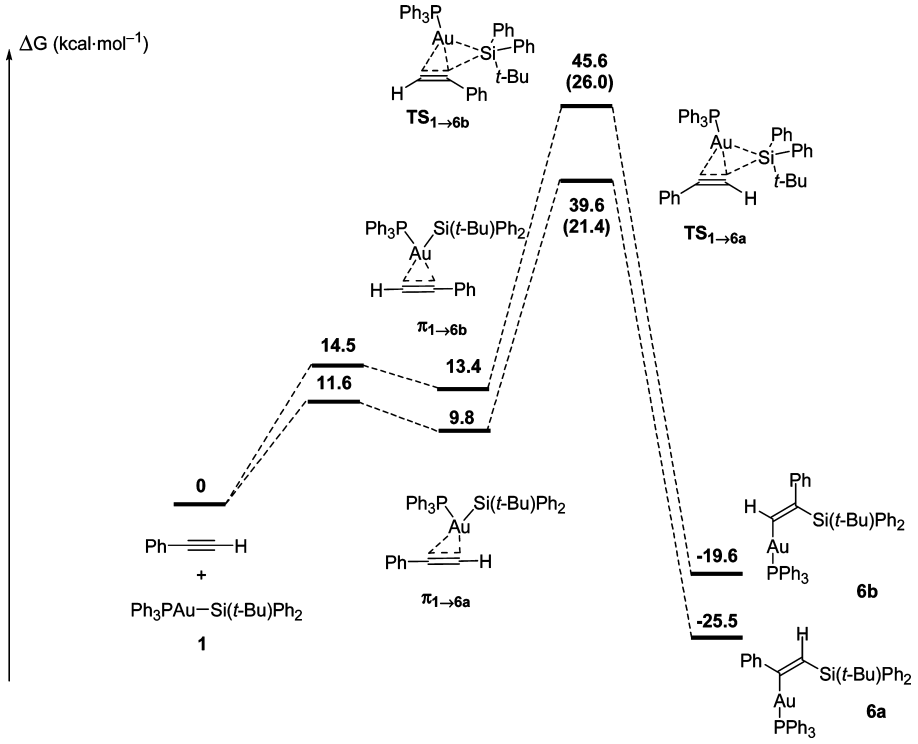

Figure 5. Reaction profiles for the formation of complexes **6a** and **6b** as the result of insertion of phenyl acetylene in the Au−Si bond of complex **1** (ΔG in kcal·mol^{-1}), computed at the B97D/SDD+f(Au)-6-31G** level of theory. Enthalpies of activation $\Delta H^{\ddagger}$ (in kcal·mol^{-1}) in parentheses.

Scheme 6. Reaction of Ethyl 2,3-Butadienoate with the Gold Silyl Complex 7

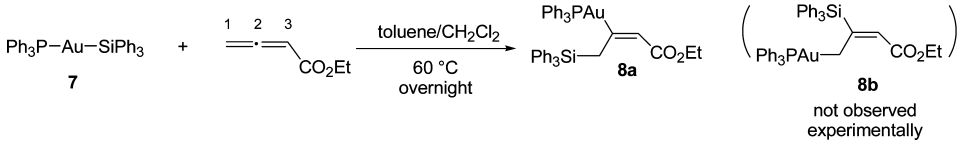

38.4 kcal·mol^{-1}), and it is very unlikely that complex **8a** is actually formed by this route.

The other transition state $\mathbf{TS}_{7\rightarrow 8b}$ adopts an out-of-plane structure. The silicon atom is tilted out of the AuC1C2 plane and approaches C2 (SiC2, 2.422 Å). In this case, the allene moiety is significantly distorted and tends to adopt planar allyl-type geometry. The terminal CH_2/$CH(CO_2Et)$ fragments are no longer perpendicular (θ = 41°), and the C1C2/C2C3 distances tend to equalize (1.411 and 1.421 Å, respectively). The gold center interacts strongly with C2 (AuC2, 2.146 Å; PAuC2, 170.9°), and the overall structure can be described as an η^1-allyl gold complex with a silyl group bridging over Au and C2. This results in a much lower activation barrier ($\Delta H^{\ddagger}_{7\rightarrow 8b}$ = −2.7 kcal·mol^{-1}, $\Delta G^{\ddagger}_{7\rightarrow 8b}$ = 17.0 kcal·mol^{-1}), suggesting that the formation of **8b** is kinetically much more favorable than that of **8a**.

Thus, in this case, the structures and energies of the two regioisomeric transition states are very different from each other. Moreover, the energy profiles computed for the formation of **8a** and **8b** are not consistent with the ready and selective formation of **8a**, as observed experimentally. To gain insights into the difference between these two insertion reactions, transition states $\mathbf{TS}_{7\rightarrow 8a}$ and $\mathbf{TS}_{7\rightarrow 8b}$ were analyzed using the activation strain model,[31,32] which enables decomposition of the activation energy $\Delta E^{\ddagger}$ into two components, the strain energy $\Delta E^{\ddagger}_{strain}$ and the interaction energy $\Delta E^{\ddagger}_{int}$. Each transition state was considered as the interaction of its constitutive fragments, i.e. the gold silyl complex and the allene. The energy required to distort each fragment from its ground-state structure to its TS geometry was estimated via single-point energy calculations ($\Delta E^{\ddagger}_{dist\text{-}AuSi}$ and $\Delta E^{\ddagger}_{dist\text{-}allene}$). The interaction energy between the two fragments $\Delta E^{\ddagger}_{int}$ was directly given by the difference between the activation energy ($\Delta E^{\ddagger}$) and the overall distortion energy $\Delta E^{\ddagger}_{strain} = \Delta E^{\ddagger}_{dist\text{-}AuSi} + \Delta E^{\ddagger}_{dist\text{-}allene}$. The results obtained for $\mathbf{TS}_{7\rightarrow 8a}$ and $\mathbf{TS}_{7\rightarrow 8b}$ are disclosed in Figure 8. The so determined interaction energy $\Delta E^{\ddagger}_{int}$ is significantly larger for $\mathbf{TS}_{7\rightarrow 8b}$ (−63.1 kcal·mol^{-1}) than for $\mathbf{TS}_{7\rightarrow 8a}$ (−48.7 kcal·mol^{-1}). This is consistent with the fact that the interaction between the two fragments is dominated by the transfer of electron density from the gold complex to the allene. And as mentioned above, the adjacent C═CH(CO_2Et) group remains a spectator in $\mathbf{TS}_{7\rightarrow 8a}$ but actively participates in $\mathbf{TS}_{7\rightarrow 8b}$ (due to the planarization of the allene framework), which contributes to the enhancement of the interaction of the gold silyl complex with the otherwise unactivated C1═C2 double bond of EB. As expected, the energy required to distort the allene is larger for $\mathbf{TS}_{7\rightarrow 8b}$ than for $\mathbf{TS}_{7\rightarrow 8a}$, but the difference is relatively small (3.8 kcal·mol^{-1}) and more than compensated by the lower distortion energy of the gold silyl complex for $\mathbf{TS}_{7\rightarrow 8b}$ than for $\mathbf{TS}_{7\rightarrow 8a}$ (11.9 kcal·mol^{-1}). Thus, both terms, the strain energy and the interaction energy, pull together and favor the formation of **8b** over **8a**.

A possibility to reconcile the reaction profiles predicted computationally and the selective formation of regioisomer **8a**

dx.doi.org/10.1021/ja504024h | J. Am. Chem. Soc. 2014, 136, 10373−10382

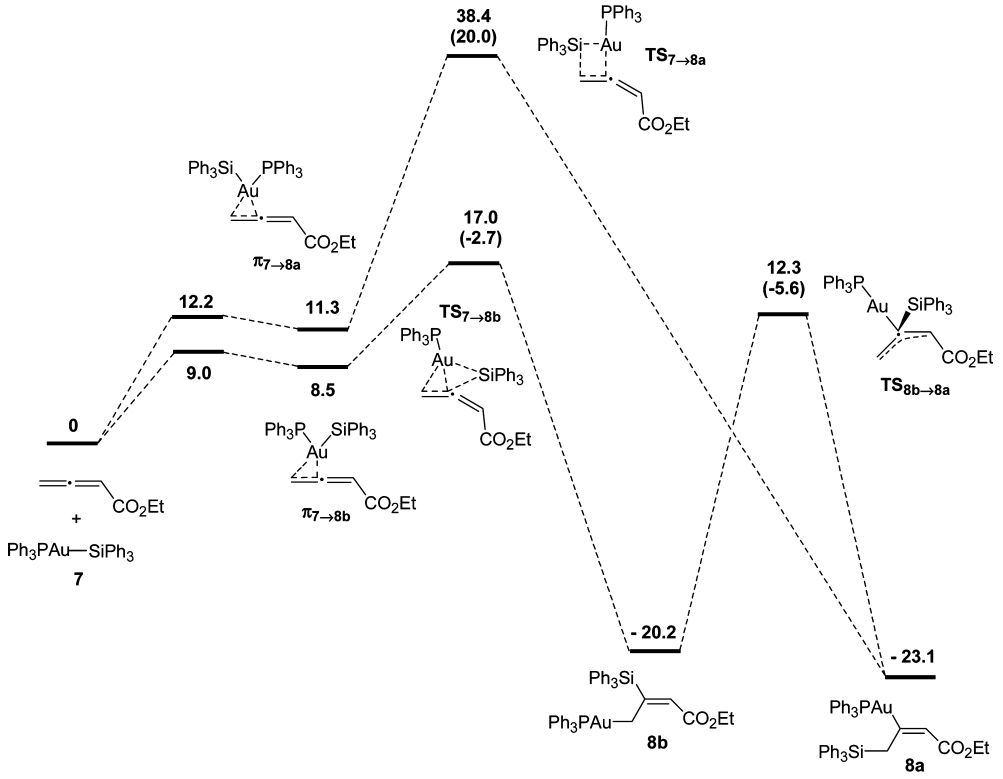

Figure 6. Two-step mechanism for the insertion of the terminal double bond of the allene into the Au–Si bond of the gold silyl complex **7** (ΔG in kcal·mol^{-1}), computed at the B97D/SDD+f(Au)-6-31G** level of theory. Enthalpies of activation $\Delta H^{\ddagger}$ (in kcal·mol^{-1}) in parentheses.

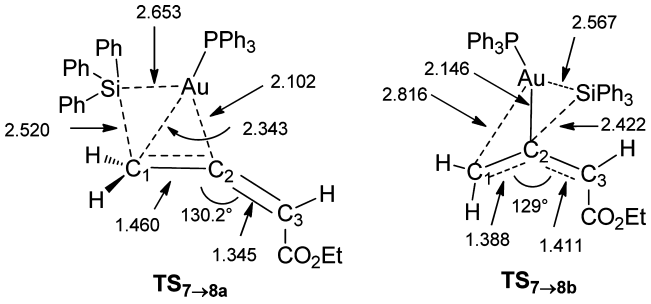

Figure 7. Main geometric features of the transition states associated with the insertion of the terminal double bond of ethyl 2,3-butadienoate in the Au–Si bond of complex **7** (B97D/SDD+f(Au)-6-31G** level of theory).

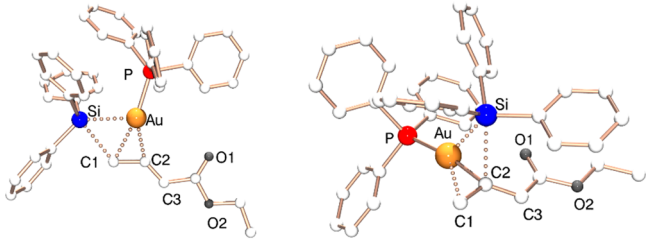

TS$_{7\rightarrow 8a}$
$\Delta\Delta G^{\ddagger} = 21.4$
$\Delta E^{\ddagger} = 18.1$
$\Delta E^{\ddagger}_{\text{dist-allene}} = 40.6$
$\Delta E^{\ddagger}_{\text{dist-AuSi}} = 26.2$
$\Delta E^{\ddagger}_{\text{int}} = -48.7$

TS$_{7\rightarrow 8b}$
$\Delta\Delta G^{\ddagger} = 0.0$
$\Delta E^{\ddagger} = -4.3$
$\Delta E^{\ddagger}_{\text{dist-allene}} = 44.4$
$\Delta E^{\ddagger}_{\text{dist-AuSi}} = 14.3$
$\Delta E^{\ddagger}_{\text{int}} = -63.1$

Figure 8. Distortion/interaction analysis of the transition states with the insertion of the terminal double bond of ethyl 2,3-butadienoate in the Au–Si bond of complex **7** (energies in kcal·mol^{-1}).

observed experimentally would likely involve the kinetically favored insertion product **8b** subsequently rearranging into the thermodynamically favored vinyl gold complex **8a**. Consistently, a transition state (**TS$_{8b\rightarrow 8a}$**) linking both products could be located on the PES. It is located only 12.3 kcal·mol^{-1} higher in energy compared to the initial reactants (and thus lower in energy than the insertion transition states **TS$_{7\rightarrow 8a}$** and **TS$_{7\rightarrow 8b}$**) and can certainly be reached under the experimental conditions (heating at 60 °C overnight). Interconversion of the alkyl and vinyl gold complexes **8b** and **8a** is a rather unusual process. **TS$_{8b\rightarrow 8a}$** corresponds to the exchange of the relative positions of gold and silicon on C1/C2, and its structure deserves comments (Figure 9). The geometry resembles that of **TS$_{7\rightarrow 8b}$**, the allene moiety being further distorted toward planar allyl-type geometry: the terminal CH_2/$CH(CO_2Et)$ fragments are rotated by only $\theta = 18°$, and the C1C2/C2C3 distances are almost identical at 1.410 and 1.433 Å, respectively. The gold

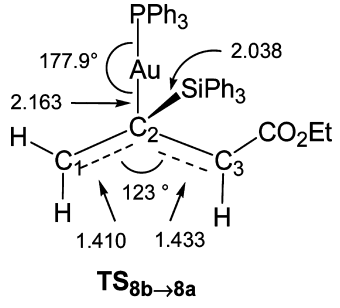

Figure 9. Main geometric features of the transition state associated with the isomerization between the gold complexes **8b** and **8a** (B97D/SDD+f(Au)-6-31G** level of theory).

dx.doi.org/10.1021/ja504024h | J. Am. Chem. Soc. 2014, 136, 10373–10382

center deviates only slightly from the plane of the C1C2C3 allyl fragment and interacts strongly with C2 (AuC2, 2.163 Å; PAuC2, 177.9°). The silicon atom also interacts mainly with C2 (2.038 Å) but sits above the η^1-allyl gold fragment, slightly tilted toward C1 (SiC1, 2.493 Å vs SiC3, 2.689 Å).

For the sake of comprehensiveness, insertion of the C2═C3 bond of EB into the Au−Si bond of complex **7** was also considered. The electron-withdrawing CO_2Et group significantly activates this double bond, the corresponding π^* orbital (which is actually the LUMO of EB) being 1.1 eV lower in energy than the $\pi^*_{C1=C2}$ (LUMO+1) orbital. Despite this electronic balance, the two conceivable π-adducts involving the C2═C3 bond of EB (Figure S32) are about isoenergetic with $\boldsymbol{\pi}_{7\rightarrow 8a}$ and $\boldsymbol{\pi}_{7\rightarrow 8b}$ involving C1═C2. This is probably due to steric shielding between the CO_2Et group at C3 and the bulky $(Ph_3P)AuSiPh_3$ fragment, which counterbalances electronic effects. Yet, insertion of the C2═C3 into the Au−Si bond was found to be less favored thermodynamically ($\Delta G_{7\rightarrow 9a} = -15.5$ kcal·mol^{-1}; $\Delta G_{7\rightarrow 9b} = -18.5$ kcal·mol^{-11}) and to require higher activation barriers ($\Delta H^{\ddagger}_{7\rightarrow 9a} = 20.5$ kcal·mol^{-1}, $\Delta G^{\ddagger}_{7\rightarrow 9b} = 41.3$ kcal·mol^{-1} and $\Delta H^{\ddagger}_{7\rightarrow 9b} = 5.7$ kcal·mol^{-1}, $\Delta G^{\ddagger}_{7\rightarrow 9b} = 25.0$ kcal·mol^{-1}). Thus, insertion of the activated C2═C3 double bond of EB is both thermodynamically and kinetically disfavored over the insertion of the terminal C1═C2 bond.

Altogether, the computational study carried out on the reaction between complex **7** and ethyl 2,3-butadienoate provides mechanistic insights and explains the rather unexpected selectivity observed experimentally. Insertion of the terminal nonactivated C═C double bond of EB into the Au−Si bond is favored and first gives the alkyl gold complex **8b**, which subsequently rearranges into the vinyl gold complex **8a** via an original Au/Si exchange process.

CONCLUSION

This comprehensive experimental/theoretical study affords a detailed mechanistic picture for the reaction of alkynes and allenes with gold silyl complexes leading to *syn* insertion products. The combination of kinetic studies, isolation and characterization of vinyl gold complexes, and DFT calculations provide evidence that the reaction is bimolecular and proceeds through a two-step coordination−insertion pathway. The π-substrates first coordinate to gold and then insert into the Au−Si bond in a *syn* fashion through a concerted inner-sphere mechanism. DFT calculations also give insight into the regioselectivity of the insertion reactions, in particular in the case of ethyl 2,3-butadienoate for which an original isomerization step (Au/Si exchange) explains the unexpected regioselectivity observed experimentally.

These studies substantiate unequivocally the ability of gold to promote the functionalization of π-substrates through an inner-sphere mechanism (alternatively to the commonly encountered outer-sphere nucleophilic addition)[15,33] and open the way to new useful chemical transformations. We are currently investigating the generality of coordination−insertion reactions at gold with the aim to increase further the versatility of this peculiar element.

ASSOCIATED CONTENT

Supporting Information

CCDC numbers for compounds **5a** and **5b**, CCDC 995108−995109, contain the supplementary crystallographic data for this paper. These data can be obtained free of charge from The Cambridge Crystallographic Data Centre via www.ccdc.cam.ac.uk/data_request/cif. Detailed experimental conditions and procedures, theoretical details, and analytical data. This material is available free of charge via the Internet at http://pubs.acs.org.

AUTHOR INFORMATION

Corresponding Authors

karinne.miqueu@univ-pau.fr
amgoune@chimie.ups-tlse.fr
dbouriss@chimie.ups−tlse.fr

Author Contributions

$^{\perp}$M.J. and L.E. contributed equally to this work.

Notes

The authors declare no competing financial interest.

ACKNOWLEDGMENTS

Financial support from the Centre National de la Recherche Scientifique, the Université de Toulouse, and the Agence Nationale de la Recherche (ANR-10-BLAN-070901) is gratefully acknowledged. The theoretical work was granted access to HPC resources of Idris under Allocation 2013 (i2013080045) made by Grand Equipement National de Calcul Intensif (GENCI). L.E. thanks the Xunta de Galicia for a postdoctoral contract under the I2C program.

REFERENCES

(1) (a) Hashmi, A. S. K.; Hutchings, G. J. *Angew. Chem., Int. Ed.* **2006**, *45*, 7896. (b) Hashmi, A. S. K. *Chem. Rev.* **2007**, *107*, 3180. (c) Li, Z.; Brouwer, C.; He, C. *Chem. Rev.* **2008**, *108*, 3239. (d) Arcadi, A. *Chem. Rev.* **2008**, *108*, 3266. (e) Gorin, D. J.; Sherry, B. D.; Toste, F. D. *Chem. Rev.* **2008**, *108*, 3351. (f) Jimenez-Nunez, E.; Echavarren, A. M. *Chem. Rev.* **2008**, *108*, 3326. (g) Fürstner, A. *Chem. Soc. Rev.* **2009**, *38*, 3208. (h) Corma, A.; Leyva-Perez, A.; Sabater, M. J. *Chem. Rev.* **2011**, *111*, 1657. (i) Boorman, T. C.; Larrosa, I. *Chem. Soc. Rev.* **2011**, *40*, 1910. (j) Bandini, M. *Chem. Soc. Rev.* **2011**, *40*, 1358. (k) Hashmi, A. S. K.; Toste, F. D. *Modern Gold Catalyzed Synthesis*, 1st ed.; Wiley-VCH Verlag GmBH & Co. KGaA: Weinheim, 2012. (l) *Acc. Chem. Res.* **2014**, issue 3; special issue edited by Friend, C. M. and Hashmi, A. S. K. on gold catalysis.

(2) For recent reviews, see: (a) Fürstner, A.; Davies, P. W. *Angew. Chem., Int. Ed.* **2007**, *46*, 3410. (b) Hashmi, A. S. K. *Angew. Chem., Int. Ed.* **2010**, *49*, 5232. (c) Liu, L. P.; Hammond, G. B. *Chem. Soc. Rev.* **2012**, *41*, 3129.

(3) For recent reviews, see: (a) Schmidbaur, H.; Schier, A. *Organometallics* **2010**, *29*, 2. (b) Brooner, R. E. M.; Widenhoefer, R. A. *Angew. Chem., Int. Ed.* **2013**, *52*, 11714.

(4) (a) Gomez-Suarez, A.; Nolan, S. P. *Angew. Chem., Int. Ed.* **2012**, *51*, 8156. (b) Braun, I.; Asiri, A. M.; Hashmi, A. S. K. *ACS Catal.* **2013**, *3*, 1902. (c) Hashmi, A. S. K. *Acc. Chem. Res.* **2014**, *47*, 864.

(5) Lein, M.; Rudolph, M.; Hashmi, A. S. K.; Schwerdtfeger, P. *Organometallics* **2010**, *29*, 2206.

(6) (a) Teles, J. H.; Brode, S.; Chabanas, M. *Angew. Chem., Int. Ed.* **1998**, *37*, 1415. (b) Krauter, C. M.; Hashmi, A. S. K.; Pernpointner, M. *ChemCatChem* **2010**, *2*, 1226.

(7) (a) Mizushima, E.; Hayashi, T.; Tanaka, M. *Org. Lett.* **2003**, *5*, 3349. (b) Nishina, N.; Yamamoto, Y. *Angew. Chem., Int. Ed.* **2006**, *45*, 3314. (c) Lavallo, V.; Frey, G.; Donnadieu, B.; Soleilhavoup, M.; Bertrand, G. *Angew. Chem., Int. Ed.* **2008**, *47*, 5224. (d) Zeng, X.; Soleilhavoup, M.; Bertrand, G. *Org. Lett.* **2009**, *11*, 3166. (e) Kinjo, R.; Donnadieu, B.; Bertrand, G. *Angew. Chem., Int. Ed.* **2011**, *50*, 5560.

(8) For addition of water and methanol to alkynes, see: Casado, R.; Contel, M.; Laguna, M.; Romero, P.; Sanz, S. *J. Am. Chem. Soc.* **2003**, *125*, 11925.

(9) For mechanistic studies of gold catalyzed hydroamination of allenes, see: Wang, Z. J.; Benitez, D.; Tkatchouk, E.; Goddard, W. A., III; Toste, F. D. *J. Am. Chem. Soc.* **2010**, *132*, 13064.

(10) The *anti* addition of amines to alkenes and allenes has been supported experimentally through labeling experiments, see: LaLonde, R. L.; Brenzovich, J.; Benitez, D.; Tkatchouk, E.; Kelley, K.; Goddard, W. A., III; Toste, F. D. *Chem. Sci.* **2010**, *1*, 226.

(11) For theoretical studies of the hydroamination of alkynes, see: (a) Kovács, G.; Lledós, A.; Ujaque, G. *Angew. Chem., Int. Ed.* **2011**, *50*, 11147. (b) Liu, X.-Y.; Guo, Z.; Dong, S. S.; Li, X.-H.; Che, C.-M. *Chem.—Eur. J.* **2011**, *17*, 12932.

(12) Theoretical investigations of gold catalyzed hydrogenation of alkenes also support an outer-sphere mechansim; see: Comas-Vives, A.; Ujaque, G. *J. Am. Chem. Soc.* **2013**, *135*, 1295.

(13) In addition, all the gold vinyl complexes isolated from the attack of nucleophiles (carboxamide, hydride, fluoride) to alkynes display a *trans* configuration; see: (a) Akana, J. A.; Bhattacharyya, K. X.; Müller, P.; Sadighi, J. P. *J. Am. Chem. Soc.* **2007**, *129*, 7736. (b) Tsui, E.; Müller, P.; Sadighi, J. P. *Angew. Chem., Int. Ed.* **2008**, *47*, 8937. (c) Hashmi, A. S. K.; Schuster, A. M.; Rominger, F. *Angew. Chem., Int. Ed.* **2009**, *48*, 8247. (d) Hashmi, A. S. K. *Gold Bull.* **2009**, *42*, 275. (e) Weber, D.; Tarselli, M. A.; Gagné, M. R. *Angew. Chem., Int. Ed.* **2009**, *48*, 5733. (f) Zeng, X.; Kinjo, R.; Donnadieu, B.; Bertrand, G. *Angew. Chem., Int. Ed.* **2010**, *49*, 942. (g) Egorova, O. A.; Seo, H.; Kim, Y.; Moon, D.; Rhee, Y. M.; Ahn, K. H. *Angew. Chem., Int. Ed.* **2011**, *50*, 11446. (h) Rosca, D.-A.; Smith, D. A.; Hughes, D. L.; Bochmann, M. *Angew. Chem., Int. Ed.* **2012**, *51*, 10643.

(14) Gold(I) amide and gold(I) phenoxide complexes have been recently isolated, and their reactivity towards alkynes has been investigated. No reaction was observed even at high temperatures, indicating that these compounds are unlikely intermediates in the insertion of π-substrates into Au−N bonds or Au−O bonds; see: (a) Johnson, M. W.; Shevick, S. L.; Toste, F. D.; Bergman, R. G. *Chem. Sci.* **2013**, *4*, 1023. (b) Oonishi, Y.; Gomez-Suarez, A.; Martin, A. R.; Nolan, S. P. *Angew. Chem., Int. Ed.* **2013**, *52*, 9767.

(15) Stradiotto et al. have reported gold catalyzed hydroamination of internal alkynes with dialkylamines. The stereo- and regioselectivity of the reactions combined with stoichiometric reactions led the authors to propose an inner-sphere insertion mechanism; see: Hesp, K. D.; Stradiotto, M. *J. Am. Chem. Soc.* **2010**, *132*, 18026. Recent mechanistic studies by Zhdanko and Maier provide further insight and point out the involvement of conformationally flexible auro-iminium salts. Accordingly, the hydroamination proceeds by outer-sphere insertion and rotation around the C−CAu bond of these auro-iminium salts is responsible for the *syn* arrangement of the final insertion products. See: (b) Zhdanko, V.; Maier, M. *Angew. Chem., Int. Ed.* **2014**, DOI: 10.1002/anie.201402557.

(16) (a) For *syn* carboauration catalyzed by Pd complexes, see: Shi, Y.; Ramgren, S. D.; Blum, S. A. *Organometallics* **2009**, *28*, 1275. (b) For two-step boraauration of terminal alkynes giving *cis* gold vinyl complexes, see: Ye, H.; Lu, Z.; You, D.; Chen, Z.; Li, Z. H.; Wang, H. *Angew. Chem., Int. Ed.* **2012**, *51*, 12047.

(17) Joost, M.; Gualco, P.; Mallet-Ladeira, S.; Amgoune, A.; Bourissou, D. *Angew. Chem., Int. Ed.* **2013**, *52*, 7160.

(18) For recent contributions involving the insertion of lakynes into Cu−Si bonds, see: (a) Fujihara, T.; Tani, Y.; Semba, K.; Terao, J.; Tsuji, Y. *Angew. Chem., Int. Ed.* **2012**, *51*, 11487. (b) Iannazzo, L.; Molander, G. A. *Eur. J. Org. Chem.* **2012**, 4923. (c) Calderone, J. A.; Santos, W. L. *Angew. Chem., Int. Ed.* **2014**, *53*, 4154. (d) Linstadt, R. T. H.; Peterson, C. A.; Lippincott, D. J.; Jette, C. I.; Lipshutz, B. H. *Angew. Chem., Int. Ed.* **2014**, *53*, 4159.

(19) Experiments in the presence of an excess of PPh_3 (0.5, 1, and 2 equiv) were also carried out to investigate the influence of added phosphine on the reaction rate. However, the addition of free phosphine resulted in the immediate polymerization of MP whatever the ratio of PPh_3. See: Simionescu, C. I.; Bulachovschi, V.; Grovu-Ivanoiu, M.; Stanciu, A. *J. Macromol. Sci., Chem.* **1987**, *A24*, 611.

(20) (a) Gomez-Gallego, M.; Sierra, A. M. *Chem. Rev.* **2011**, *111*, 4857. (b) Weiss, C. J.; Marks, T. J. *J. Am. Chem. Soc.* **2010**, *132*, 10633. (c) Weiss, C. J.; Wobser, S. D.; Marks, T. J. *Organometallics* **2010**, *29*, 6308. (d) Arndt, M.; Salih, K. S. M.; Fromm, A.; Goossen, L. J.; Menges, F.; Niedner-Schatteburg, G. *J. Am. Chem. Soc.* **2011**, *133*, 7428.

(21) Grimme, S. *J. Comput. Chem.* **2006**, *27*, 1787.

(22) Grimme, S.; Diedrich, C.; Korth, M. *Angew. Chem., Int. Ed.* **2006**, *45*, 625.

(23) For discussions on the difficult estimation of entropic efffects with multimolecular processes, see: Braga, A. A. C.; Ujaque, G.; Maseras, F. *Organometallics* **2006**, *25*, 3647.

(24) The only TS connecting **1** + DMAD and **5b** located on the PES is associated with direct 1,2-addition (in-plane four-membered ring TS). But the corresponding activation barrier ($\Delta G^{\ddagger}$ = 52.6 kcal·mol^{-1}) is prohibitively high and the formation of **5b** is very unlikely to result from this process (Figure S27).

(25) For discussions on phosphine dissociation from gold, see: Kumar, M.; Jasinski, J.; Hammond, G. B.; Xu, B. *Chem.—Eur. J.* **2014**, *20*, 3113.

(26) Phosphines are known to readily react with electron-poor alkynes to give zwitterionic phosphonium enolates. See for example: Zhu, X.-F.; Henry, C. E.; Kwon, O. *J. Am. Chem. Soc.* **2007**, *129*, 6722.

(27) The direct 1,2-addition pathway is associated with a much higher activation barrier ($\Delta G^{\ddagger}$ = 38.4 kcal·mol^{-1}), and the two-step mechanism involving phosphine dissociation/1,2-addition/phosphine association requires an even higher activation barrier ($\Delta G^{\ddagger}$ = 55.1 kcal·mol^{-1}) (Figure S29).

(28) A similar situation was reported for the *trans*-[$PtCl(SiMePh_2)(PMe_2Ph)_2$] complex. Due to the *trans* influence of the silyl group, the Pt−Cl distance is elongated by about 0.15 Å compared to that of $(PtCl_4)^{2-}$; see: Kapoor, P.; Lövqvist, K.; Oskarsson, Å. *Acta Crystallogr.* **1995**, *C51*, 611.

(29) For leading contributions on the gold chemistry of allenes, see: (a) Gandon, V.; Lemière, G.; Hours, A.; Fensterbank, L.; Malacria, M. *Angew. Chem., Int. Ed.* **2008**, *47*, 7534. (b) Malacria, M.; Fensterbank, L.; Gandon, V. *Top. Curr. Chem.* **2011**, *302*, 157. (c) Montserrat, S.; Ujaque, G.; Lopez, F.; Mascarenas, J. L.; Lledos, A. *Top. Curr. Chem.* **2011**, *302*, 225. (d) Krause, N.; Winter, C. *Chem. Rev.* **2011**, *111*, 1994. (e) Montserrat, S.; Faustino, H.; Lledos, A.; Mascarenas, J. L.; Lopez, F.; Ujaque, G. *Chem.—Eur. J.* **2013**, *19*, 15248. (f) Yang, W.; Hashmi, A. S. K. *Chem. Soc. Rev.* **2014**, *43*, 2941.

(30) A similar two-step mechanism has been computed for palladium-catalyzed sila-stannation of allenes; see: Wang, M.; Cheng, L.; Hong, B.; Wu, Z. *J. Comput. Chem.* **2009**, *30*, 1521.

(31) For selected mechanistic computational studies including distortion/interaction analyses, see: (a) Ess, D. H.; Houk, K. N. *J. Am. Chem. Soc.* **2007**, *129*, 10646. (b) Ess, D. H.; Houk, K. N. *J. Am. Chem. Soc.* **2008**, *130*, 10187. (c) Hong, X.; Liang, Y.; Houk, K. N. *J. Am. Chem. Soc.* **2014**, *136*, 2017. (d) Green, A. G.; Liu, P.; Merlic, C. A.; Houk, K. N. *J. Am. Chem. Soc.* **2014**, *136*, 4575.

(32) van Zeist, W.-J.; Bickelhaupt, F. M. *Org. Biomol. Chem.* **2010**, *8*, 3118.

(33) For *cis*-disilylation and silaboration of alkynes catalyzed by supported gold nanoparticles, see: (a) Gryparis, C.; Kidonakis, M.; Stratakis, M. *Org. Lett.* **2013**, *15*, 6038. (b) Gryparis, C.; Stratakis, M. *Org. Lett.* **2014**, *16*, 1430.